

Direct observation of topological Hall effect in Co/Pt nanostructured filmsM. V. Sapozhnikov ^{1,2,*}, N. S. Gusev,¹ S. A. Gusev ¹, D. A. Tatarskiy,^{1,2} Yu. V. Petrov,³
A. G. Temiryazev ⁴ and A. A. Fraerman¹¹*Institute for Physics of Microstructures RAS, Nizhny Novgorod, 603950, Russia*²*Lobachevsky State University of Nizhny Novgorod, 603950 Nizhny Novgorod, Russia*³*Physics Department, Saint Petersburg State University, Saint Petersburg, Russia*⁴*Kotelnikov Institute of Radioengineering and Electronics RAS, Fryazino Branch, Fryazino, Russia* (Received 10 May 2020; revised 1 February 2021; accepted 3 February 2021; published 19 February 2021)

A method consisting of simultaneous measurements of a Hall effect and a magneto-optic Kerr effect is used to study a topological Hall effect in thin ferromagnetic films. The method is based on the idea that the values of the topological effects are different at dc and optical frequencies. The topological Hall effect in the artificial lattices of magnetic bubbles in nanostructured Co/Pt multilayers with perpendicular magnetic anisotropy is investigated using this method. The Lorentz transmission electron microscopy measurements demonstrate skyrmionic topology of the magnetic bubbles. The measured topological Hall effect is proportional to the skyrmion density in the system.

DOI: [10.1103/PhysRevB.103.054429](https://doi.org/10.1103/PhysRevB.103.054429)

A topological Hall effect (THE) arises from the Berry phase acquired by an electron moving in a non-coplanar varying magnetic field [1]. In the case of electrons in ferromagnetic material with non-coplanar distribution of magnetization it is a transversal transport effect of the exchange nature [2], while the well-known giant magnetoresistance is a longitudinal transport exchange effect [3]. The experimental observation of the THE became much more feasible after the discovery of magnetic skyrmions [4,5]. The skyrmions are swirling noncoplanar spin textures with nonzero topological charge [6], which are soliton-like solutions for magnetization in materials with uniaxial anisotropy [7]. The THE was experimentally observed in the skyrmionic *A* phase of the chiral magnet MnSi [8] where it is stabilized by the Dzyaloshinskii-Moriya interaction (DMI). To date the THE in chiral magnetic materials is reported in a number of works. The first observations of the THE in transitional ferromagnetic metal films on the surface of a heavy-metal sublayer are demonstrated in [9,10]. The THE is observed as an additional contribution in Hall measurements superposed on the ordinary and the extraordinary (anomalous) Hall effects (AHE) [11–13]. The problem is that it is impossible to measure the THE separately. The ordinary Hall effect can be measured at high fields and then subtracted from the Hall hysteresis loop. To divide the THE and AHE they usually assume some form of AHE hysteresis *a priori* and then subtract this assumed AHE from the experimental curve. This procedure is a weak point of most of the THE measurements “on the market” and leads to a criticism in some later works. It is demonstrated that the features of the Hall effect usually attributed to the THE can be explained in the framework of AHE [14,15]. So there is still a problem of the interpretation of the THE measurements.

In the case of bulk materials, the THE effect can be extracted by comparing Hall loop and magnetization loop measured with a magnetometer. For ultrathin films they compare the Hall effect and magneto-optic Kerr effect (MOKE), assuming that the magnitude of the Kerr signal is proportional to the magnetization [16,17]. This assumption is not obvious. Before using the MOKE to measure the magnetization of a system, it is necessary to estimate the value of the topological component of this effect.

In this work, we raise the question of the possible dependence of the topological effect on frequency. At first we estimate the value of the topological effect in magneto-optics and show that it is negligible in the optical range. Then we use the method of simultaneous measurements of the Hall effect and the magneto-optical Kerr effect to study the THE in artificial lattices of magnetic bubbles in nanostructured Co/Pt multilayers. Due to a sophisticated method of nanomodification of the films the magnetic bubbles can become skyrmions in the magnetization process. The skyrmionic topology of the magnetic bubbles is verified by Lorentz transmission electron microscopy (LTEM) measurements. Our methods make it possible to create skyrmion lattices of a predetermined density. The experimental difference in the normalized Hall and MOKE signals is interpreted as the THE. The observed THE value is proportional to the density of the topological charge in the system.

Estimation of topological magneto-optic effect. Phenomenologically both the magneto-optic Kerr effect and the Hall effect are described by the off-diagonal components of the permittivity tensor. According to the Onsager reciprocal relations for kinetic coefficients, these components are odd functions of the magnetization \mathbf{M} . In a homogeneous magnetic medium the permittivity tensor is proportional to the magnetization. In an inhomogeneous non-coplanar magnetic medium, an additional contribution to the off-diagonal components of the permittivity appears, due to the existence of a

*Corresponding author: msap@ipmras.ru

“hidden” topological magnetic field. The expression for the permittivity tensor components describing the Kerr and Hall effects takes the form

$$\varepsilon_{i,k}(\mathbf{M}) = \alpha(\omega)\varepsilon_{ikl}M_l + \beta(\omega)\left(\mathbf{M}\left[\frac{\partial\mathbf{M}}{\partial x_i} \times \frac{\partial\mathbf{M}}{\partial x_k}\right]\right). \quad (1)$$

Here ε_{ikl} is Levi-Civita symbol. The first term describes linear magneto-optic effects and anomalous dc Hall effect (at $\omega \rightarrow 0$). The second term corresponds to the topological contribution to the Hall and Kerr effects. The phenomenological coefficients $\alpha(\omega)$ and $\beta(\omega)$ describe the frequency dispersion of these effects. So from a symmetry point of view the topological MOKE should also exist.

The initial theoretical approach to the THE is based on the assumption that the inverse transit time of the electron through magnetic inhomogeneity τ^{-1} is less than the frequency ω_R of quantum transitions between two electron spin sublevels split by the exchange interaction with localized magnetic moments. The adiabatic approximation is applicable in this situation [1,2,18]. The calculated topological correction to the Hall effect is proportional to the effective field $B = \Phi_0\psi$, where $\Phi_0 = hc/e_0$ is the magnetic flux quantum and $\psi = \frac{1}{4\pi}(\mathbf{n}[\frac{\partial\mathbf{n}}{\partial x} \times \frac{\partial\mathbf{n}}{\partial y}])$ is the local density of the topological charge of the magnetization distribution ($\mathbf{n} = \mathbf{M}/M$ is the magnetization direction vector). The adiabatic approximation corresponds to the dc current through skyrmions in Co/heavy-metal systems where skyrmion size is more than 50 nm. The opposite situation when $\omega_R\tau \leq 1$ corresponds to materials with smaller skyrmions and relatively weak exchange interaction. In this case the adiabatic approximation is not applicable and the problem can be solved by perturbation methods [19,20]. So adiabatic and nonadiabatic regimes can be realized in the systems with different material parameters and with different ratios of these characteristic times.

The system of classical equations describing the THE consists of Newton’s equation for an electron moving in an exchange field and the Landau-Lifshitz equation for its magnetic moment [1]. These equations are obtained in the approximation of adiabaticity ($\omega_R\tau > 1$) and quasiclassicality ($ak > 1$, where a is the scale of the magnetic inhomogeneity and k is the wave number of an electron). Consider this model by adding a weak alternating electric field to Newton’s equation as a correction. A rigorous justification of such a generalization is beyond the scope of this work and is the subject of a separate theoretical study. We only note that the introduction of a uniform electric field leaves the quasiclassical approximation valid:

$$m_0 \frac{\partial^2 x_i}{\partial t^2} = \gamma \mathbf{J} \mathbf{S} \frac{\partial \mathbf{M}}{\partial x_i} + e_0 E_i e^{-i\omega t}, \quad (2)$$

$$\frac{\partial \mathbf{S}}{\partial t} = \gamma J [\mathbf{S} \times \mathbf{M}], \quad (3)$$

where e_0 , m_0 , and S are electron charge, mass, and internal angular momentum. \mathbf{M} is magnetization, J is the dimensionless exchange constant, and γ is the gyromagnetic ratio. The first term in (2) is supposed to be small. In this case the oscillating electron is in an alternating field of the magnetization,

$$\mathbf{M} \approx \mathbf{M}_0 + (\mathbf{r}\nabla)\mathbf{M} = \mathbf{M}_0 - (\mathbf{E}\nabla)\mathbf{M} \frac{e_0}{\omega^2 m_0} e^{-i\omega t}. \quad (4)$$

Such representation is valid, as the amplitude of electron displacement is small due to high frequency. Let us find the solution of (3) in the standard form

$$\mathbf{S}(t) = \mathbf{S}_0 + \mathbf{s} e^{-i\omega t}, \quad (5)$$

where $\mathbf{s} \ll \mathbf{S}$. In the case when $\omega \gg \omega_R = \gamma J M_0$ the solution can be found (see [21], for example) in the form of

$$\begin{aligned} \mathbf{s} &= \frac{i e_0 S_0}{\gamma J M_0 m_0 \omega} \left(\frac{\omega_R}{\omega}\right)^2 [\mathbf{M} \times (\mathbf{E}\nabla)\mathbf{M}] e^{-i\omega t} \\ &= A [\mathbf{M} \times (\mathbf{E}\nabla)\mathbf{M}]. \end{aligned} \quad (6)$$

The constant

$$A = \frac{i e_0 S_0}{\gamma J M_0 m_0 \omega} \left(\frac{\omega_R}{\omega}\right)^2 \quad (7)$$

is introduced for brevity. $\omega_R = 5 \times 10^{13}$ to 5×10^{14} Hz is the frequency of the electron magnetic moment precession in the exchange field. It is 10–100 times less than optical frequency. Now it is possible to find the exchange force in (2) taking into account that $\mathbf{S}_0 \parallel \mathbf{M}_0$:

$$\begin{aligned} F_i &= \gamma J S_k \frac{\partial M_k}{\partial x_i} = \gamma J A \left[\mathbf{M} \times \left(E_j \frac{\partial \mathbf{M}}{\partial x_j} \right) \right]_k \frac{\partial M_k}{\partial x_i} \\ &= \gamma J A \varepsilon_{ksq} M_s E_j \frac{\partial M_q}{\partial x_j} \frac{\partial M_k}{\partial x_i} \\ &= - \frac{i e_0 S_0}{m_0 \omega} \left(\frac{\omega_R}{\omega}\right)^2 E_j e^{-i\omega t} \left(\mathbf{n} \left[\frac{\partial \mathbf{n}}{\partial x_j} \frac{\partial \mathbf{n}}{\partial x_i} \right] \right). \end{aligned} \quad (8)$$

Here ε_{ksq} is the Levi-Civita symbol, and $\mathbf{n} = \mathbf{M}/M$ is the magnetization direction vector. Let us take into account that electron velocity is $V_j = i e_0 E_j e^{-i\omega t} / m_0 \omega$ and $S_0 = \hbar/2$. In its turn $(\mathbf{n}[\frac{\partial\mathbf{n}}{\partial x_j} \frac{\partial\mathbf{n}}{\partial x_i}]) = 4\pi\psi\varepsilon_{ijk}b_k$, where \mathbf{b} is a unit vector, and ψ is a local density of the topological charge of the magnetization distribution. Thus the founded force can be rewritten as

$$F_i = (e_0/c)\Phi_0\psi(\omega_R/\omega)^2\varepsilon_{ijk}V_j b_k, \quad (9)$$

where $\Phi_0 = hc/e$ is the magnetic flux quantum. Evidently \mathbf{F} has the form of the Lorentz-type force with effective field

$$B = \Phi_0\psi(\omega_R/\omega)^2. \quad (10)$$

The additional factor $(\omega_R/\omega)^2$ appears in the comparison with the dc THE. The topological magneto-optic rotation of the electromagnetic wave polarization should be resonantly high at the frequencies corresponding to the energy of the exchange interaction and noticeable in the infrared band. In the optic band $\omega_R/\omega \sim 10^{-1}$ to 10^{-2} and the magneto-optic topological effect is negligible in comparison with the dc THE. So the direct comparison of optical band Kerr and dc Hall effect loops can be used to subtract the THE.

Experimental methods and samples. A measuring home-built system is developed to obtain the MOKE and Hall effect hysteresis loops of the samples in the same run. This ensures that the MOKE and Hall data are obtained for the same magnetization configuration of the system. Thin Co/Pt multilayered samples [5 alternating Co (0.5 nm thick) and Pt (1 nm thick) layers grown by dc magnetron sputtering] have

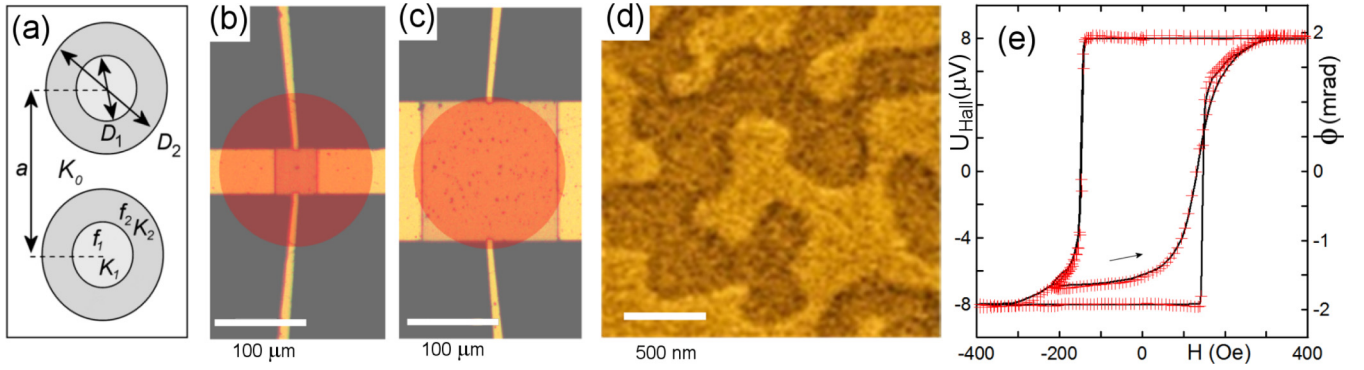


FIG. 1. (a) The geometry of nanomodification: the irradiated spots with the reduced anisotropy form a rectangular lattice with the period of a ; D_1 and D_2 are the diameters of the concentric regions with different irradiation fluence (f_1 and f_2 , correspondingly) and anisotropy (K_1 , K_2). (b) Photo of the $50 \times 50 \mu\text{m}^2$ Hall cross; the red circle depicts the visible spot size of the focused laser beam. (c) The same for the $150 \times 150 \mu\text{m}^2$ Hall cross. (d) The MFM image of the labyrinth domain structure of the initial Co/Pt film in the demagnetized state. (e) The Hall (black line) and polar MOKE (red crosses) hysteresis loops of the initial Co/Pt film plotted on the same scale. A minor loop is also presented.

a square form with attached golden current and voltage leads. Two identical series of the samples which differ only by sizes of Hall crosses [$50 \times 50 \mu\text{m}^2$ and $150 \times 150 \mu\text{m}^2$; Figs. 1(b) and 1(c)] are fabricated for comparison. The current in the Hall bridge is $50 \mu\text{A}$. MOKE measurements are done in the polar geometry ($\lambda = 632 \text{ nm}$). The laser beam is focused on the Hall cross; the visible light spot diameter is $\sim 150 \mu\text{m}$. Experimental data are taken as a function of magnetic field to generate MOKE and Hall hysteresis loops in the same run. This helps us to avoid artifacts resulting from using different measurement setups. The samples are thin enough (total thickness is 7.5 nm) that the entire volume of the sample contributes to the MOKE signal. All experiments are carried out at room temperature.

The samples are nanostructured using the focused He^+ ion beam irradiation technique described in detail in Ref. [23] to form a rectangular lattice of the nanospots with radially dependent reduced perpendicular anisotropy. The central part of a spot is irradiated with a smaller fluence. This reduces the anisotropy value but the anisotropy remains of the easy-axis type. The peripheral area is irradiated with higher fluences to form narrow concentric ring-shaped area with easy-plane type anisotropy [Fig. 1(a)]. We choose the necessary fluences according to [22]. The parameters of the samples are summarized in Table I. Such sophisticated nanostructuring allows us to artificially form the dense uniform lattices of magnetic

TABLE I. Parameters of the samples. D_1 and f_1 are the diameter and the fluence of the central part of an irradiated spot [Fig. 1(a)], D_2 and f_2 are the same for the outer ringed region, a is the lattice period, and ψ is density of magnetic bubbles.

No.	D_1 (nm)	f_1 (cm^{-2})	D_2 (nm)	f_2 (cm^{-2})	a (nm)	ψ_{max} (μm^{-2})
1	180	2×10^{15}	200	4×10^{15}	300	11
2	80	2×10^{15}	100	4×10^{15}	160	39
3	60	2×10^{15}	100	4×10^{15}	200	25
4	100	2×10^{15}			200	25

bubbles which can become skyrmions in the magnetization process. The lattices with different periods are obtained. This facilitates the observation of the THE in the system. The formation of the skyrmions in such systems was previously predicted by micromagnetic calculations [23,24].

We should note here that the initial unpatterned Co/Pt film demonstrates rectangular hysteresis loops which is typical for magnetic film with perpendicular easy-axis anisotropy without any noticeable difference between MOKE and Hall curves [Fig. 1(e)]. In the demagnetized state the film exhibits a labyrinth domain structure [Fig. 1(d)].

We used magnetic force microscopy (MFM) to visualize magnetic states, existing at zero field. A phase shift of the probe oscillations is registered as an MFM signal. Small voltage is applied to the probe to compensate the tip-sample contact potential difference and reduce the electrostatic interaction [25]. MFM cannot resolve a topological structure of appearing magnetic bubbles but it allows us to verify uniformity of the obtained domain lattices, to estimate the density of the bubble domains, and to distinguish magnetic vortices from magnetic bubbles [22].

The topology of magnetization distribution in the appearing magnetic bubbles is examined by Lorentz transmission electron microscopy (LTEM) measurements [26]. The C_s -corrected transmission electron microscope TITAN 80-300 (FEI) operated at 300 kV is used. The overfocused conditions (defocus value 3 mm) are used to increase Fresnel contrast of the LTEM images [27]. The spatial resolution of the method is approximately 70 nm . The special Co/Pt nanostructured samples are prepared on commercial Si_3N_4 50 nm thick membranes for these measurements. The diameters of the irradiated concentric spots are increased to 300 and 400 nm for better resolution.

Experimental results. The principal experimental result is represented in Fig. 2 for sample 1. The Hall and MOKE curves are very similar in general. Nevertheless there is one noticeable difference between them. Namely it is an additional step in the Hall curve at $H \approx -200 \text{ Oe}$ which is absent in the MOKE curve. Both the MOKE and AHE are linearly proportional to the magnetization. So it is possible to calculate

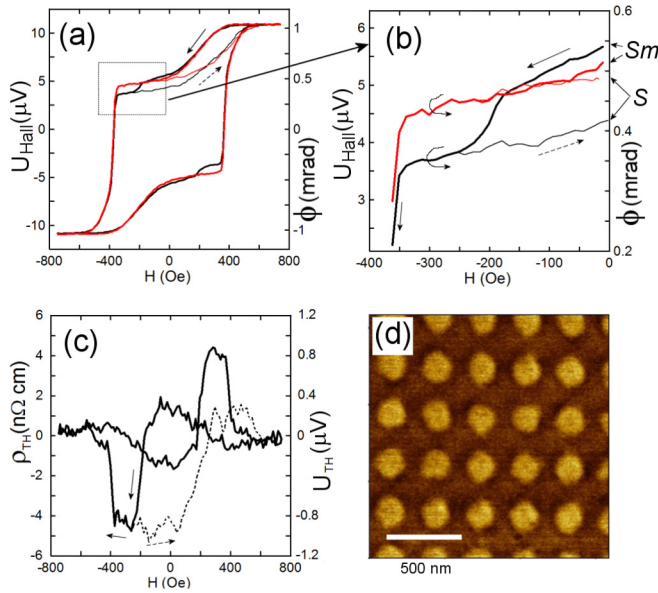


FIG. 2. Experimental data for sample 1 ($50 \times 50 \mu\text{m}^2$ Hall cross), Table 1: (a) MOKE (red line) and Hall (black line) hysteresis loops plotted on the same scale. Thinner lines are for minor loops. (b) The close view of the step in the Hall curve. Letters “Sm” and “S” correspond to the skyrmionium lattice (remanent state) and skyrmion lattice. (c) The hysteresis curve of the topological Hall effect. Dotted line is for minor loop. (d) MFM image of the system in the remanent state [corresponding to point Sm in (b)].

the THE by subtracting the properly scaled MOKE curve from the Hall curve. The following procedure is used. Taking into account the small value of the ordinary Hall effect in Co in a field equal to the saturation field (~ 500 Oe) and the absence of the THE in a uniformly magnetized state, we determine the proportionality coefficient between the AHE signal and the MOKE. Since a topological MOKE is negligible, the MOKE is proportional to the magnetization of the system. This allows the AHE loop to be restored from the MOKE loop. Subtracting the AHE loop from the total Hall effect loop, we obtain the dependence of the THE on the external magnetic field. The result is represented in Fig. 2(c). The corresponding step in the Hall resistance has a value of $\Delta \sim 4 \text{ n}\Omega \text{ cm}$.

The general form of the MOKE and Hall loops of sample 2 (Fig. 3) is different in comparison with the curves of sample No. 1. But what is really important is that the second sample demonstrates a similar step in the Hall effect [Fig. 3(b)] which is absent in the MOKE [Fig. 3(a)]. To make the difference more evident we plot the same minor hysteresis loops in both figures. The THE is more pronounced in the second sample; the step in the Hall signal has a value of $\Delta \sim 15 \text{ n}\Omega \text{ cm}$.

Figure 4 shows the loops for sample 3. The difference of the MOKE and the Hall loops is visible for this sample too. This difference corresponds to the THE value and is equal to $\Delta \sim 10 \text{ n}\Omega \text{ cm}$.

The MFM measurements demonstrate dramatic change in the magnetic states of the nanostructured samples compared with the initial unstructured film. The irradiated spots show individual magnetic contrast in this case. The MFM signal has radial symmetry within the spot, which indicates

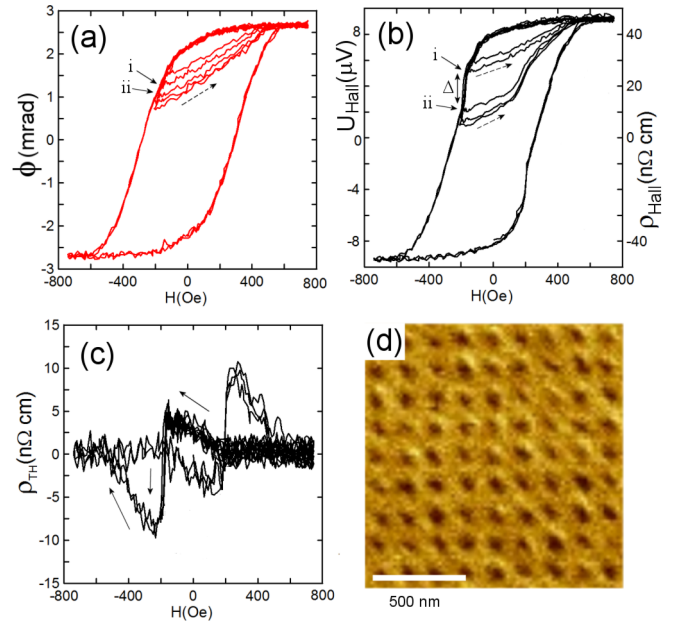


FIG. 3. Experimental data for sample 2 ($50 \times 50 \mu\text{m}^2$ Hall cross): (a) MOKE hysteresis loop. (b) Hall hysteresis loop. Points denoted by “i” and “ii” are the same for Hall and MOKE loops. (c) The hysteresis curve of the topological Hall effect; lines corresponding to minor loops are not represented. (d) MFM image of the dense lattice of magnetic bubbles in the remanent state.

the radial symmetry of the magnetization distribution; we do not observe magnetic poles of the different sign within the same spot. In the remanent state, each irradiated point contains a magnetic bubble. Thus, the formation of dense regular lattices of magnetic bubbles is observed in all samples [Figs. 2(d), 3(d), 4(a)]. Note that MFM imaging in saturation magnetic field does not show any contrast. Thus, we conclude that neither the magnitude of the magnetization nor the surface potential changes are in the irradiation spots.

The study of the topology of the magnetization distribution in the magnetic bubbles in the demagnetized state [point “S” in Fig. 2(b)] is carried out by LTEM methods. The results are shown in Fig. 5. It can be seen that the cores of the domains are surrounded by circular Bloch domain walls that do not contain

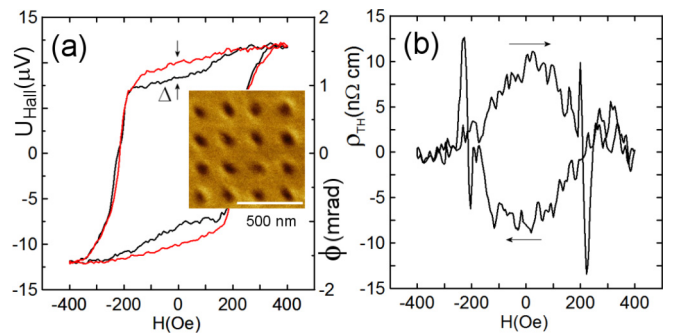


FIG. 4. (a) MOKE (red line) and Hall (black line) hysteresis loops plotted on the same scale for sample 4 ($50 \times 50 \mu\text{m}^2$ Hall cross). Inset: MFM image in the remanent state. (b) Hysteresis curve of the topological Hall effect.

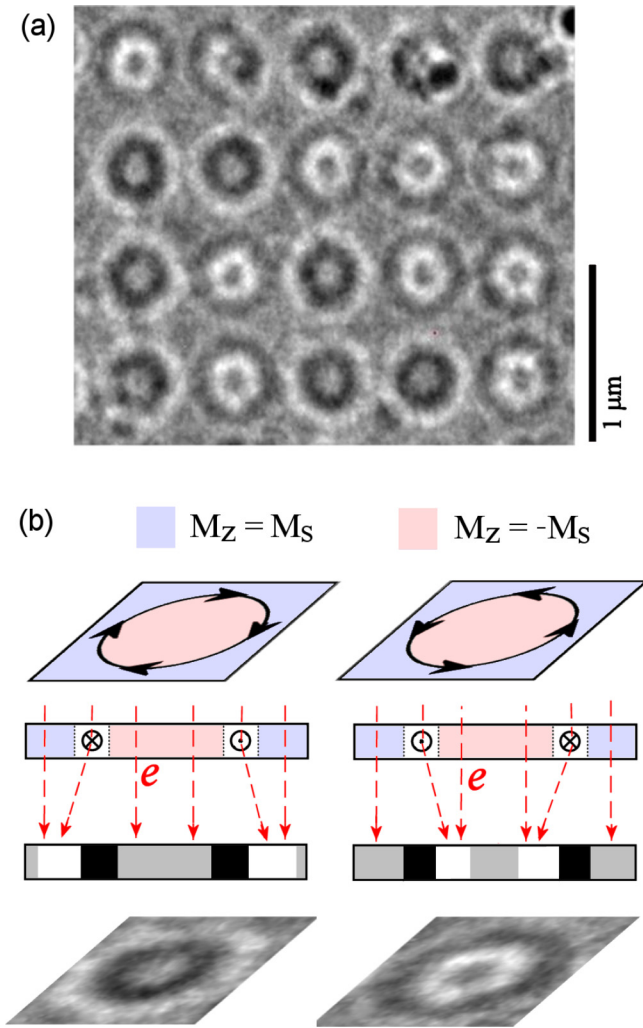


FIG. 5. (a) LTEM image of a lattice of magnetic bubbles in a demagnetized state. The observed contrast corresponds to the distribution of magnetization for Bloch skyrmions. It is observed from the skyrmion with both right and left helicity. (b) Schematic representation of the formation of LTEM images for skyrmions with different helicity.

Bloch lines. The possible presence of the Néel component in the domain wall does not affect the formed LTEM image and cannot be verified. Thus, from the topology point of view, the magnetic bubbles formed in the demagnetized state are skyrmions. The sign of the topological charge of a skyrmion does not depend on its helicity. Accordingly, the contribution of right and left twisted skyrmions to the observed effects must be additive. The number of skyrmions with right and left helicity approximately coincides, which confirms the absence of the bulk DMI in the samples under study.

We should note that the measured MOKE and Hall loops for the samples of $150 \times 150 \mu\text{m}^2$ and $50 \times 50 \mu\text{m}^2$ are identical. This means that the possible nonuniformity of the laser irradiation or current distribution in the Hall bar do not affect the obtained results.

Discussion. The problem of the magnetization reversal in the system under study is theoretically examined in Refs. [23,24] in detail. A possible sequence of the magnetic

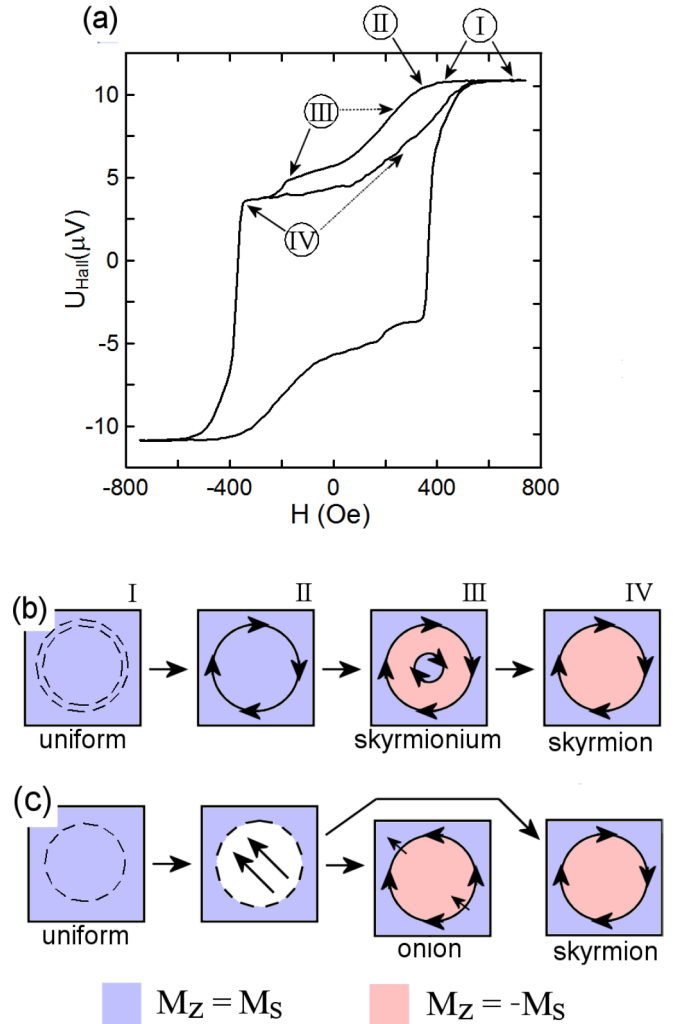


FIG. 6. (a) Hall hysteresis loop of sample 1. The numbers indicate the parts of the loop corresponding to the different magnetic states of the system. (b), (c) Schematic sequence of the magnetization states in the samples during magnetization reversal. Arrows denote direction of in-plane magnetization; colors denote direction of perpendicular magnetization. Dotted circles represent schematically the irradiated areas [see also Fig. 1(a)]. (b) Concentric distribution of the anisotropy value in the spot (samples 1, 2, and 3). (c) Uniformly decreased anisotropy value in the spot (sample 4).

states in the system appearing during the magnetization reversal process, which can explain the observed MOKE and Hall hysteresis loops, is schematically represented in Fig. 6. The formation of skyrmions in the system is facilitated by the specially designed shape of the irradiated areas. The outer concentric ring [Fig. 1(a)] has easy-plane anisotropy while other areas of the film have easy-axis anisotropy. The results of micromagnetic simulations of the system allow us to assume that the scenario of magnetization reversal of the system might be the following. With a decrease of the external field the magnetization reversal of the saturated state in the system begins with the tilting of the magnetization in the ring resulting in formation of magnetic bubbles. At this moment the bubbles have the topology of the skyrmionium. Actually, the “skyrmionium” is a topologically trivial state, which can

be considered as a pair of concentric magnetic skyrmions with opposite topological charges [28,29]. As a trivial state it does not cause the THE. Further decrease of the magnetic field leads to collapse of the central core of the skyrmionium and its transformation into the topologically charged skyrmion. As the volume of the cores is sufficiently small at this moment, the magnetization of the system changes negligibly, so there is no step in the MOKE curve of the system. At that, the dense skyrmion lattice appearing at this moment carries the topological charge equal to the density of the irradiated spots ψ . This is accompanied by the emergence of the THE leading to the step appearance in the Hall curve. If at this point the magnetic field is returned to zero, the skyrmions remain stable and the THE contribution remains, leading to the difference in the main and minor Hall loops at the zero field [points “Sm” and “S” in Fig. 2(b)].

At the same time the minimal difference between the MOKE signal in the Sm and S points in Fig. 2(b) allows us to conclude that the central core of the skyrmionium takes small volume at the zero external field. Therefore the MFM images of the skyrmionium lattice state [Fig. 2(d)] and skyrmion lattice state are actually the same, as the MFM technique does not allow us to resolve the small central core of the skyrmionium in this case. With the increase of the magnetic field the “skyrmionium” (upper) branch and “skyrmion” (lower) branch of the MOKE curve diverge from each other as the central cores of the skyrmioniums expand and begin to noticeably contribute to average perpendicular magnetization.

The experimentally observed general difference in the loops of samples 1 (Fig. 2) and 2 (Fig. 3) exists because the samples have different geometry and so different magnetostatic interaction between and inside appearing skyrmioniums. The irradiated spots in the case of sample 3 take 20% of the whole surface of the film. This is less than in the two previous samples (35% and 30%). The smaller size of the skyrmionium states or larger distance between them increases their magnetostatic energy and makes them less stable. Therefore, topologically charged skyrmions appeared earlier—already in $H \approx +100$ Oe. So, even in the remanent state we have the dense skyrmion lattice and the difference in the MOKE and Hall curves for the third sample.

It is remarkable that measured value of the THE is proportional to the density of skyrmions [Fig. 7(d)] appearing in the irradiated spots (see Table I). This additionally confirms that the observed effect is indeed the THE. The measured THE value is ≈ 0.4 n Ω cm per skyrmion/ μm^2 .

This value is qualitatively close to the values measured in other films of transition ferromagnetic metals, which are 0.6 n Ω cm per skyrmion/ μm^2 measured for the THE in Ir/Fe/Co/Pt multilayers [10] and 0.67 n Ω cm per skyrmion/ μm^2 measured for the THE in Pt/Co/Ta films [9]. Due to the strong DMI in these structures, the size of skyrmions is slightly smaller compared with our samples and is ~ 50 nm.

If we consider chiral B20 materials, then FeGe is closest to transition ferromagnetic metals in its properties. The skyrmions in it have the same typical size of ~ 40 nm and are stable at nearly room temperature [30]. Due to the sufficiently large size of skyrmions, the adiabatic condition for electron current is satisfied for it, as well as for transition

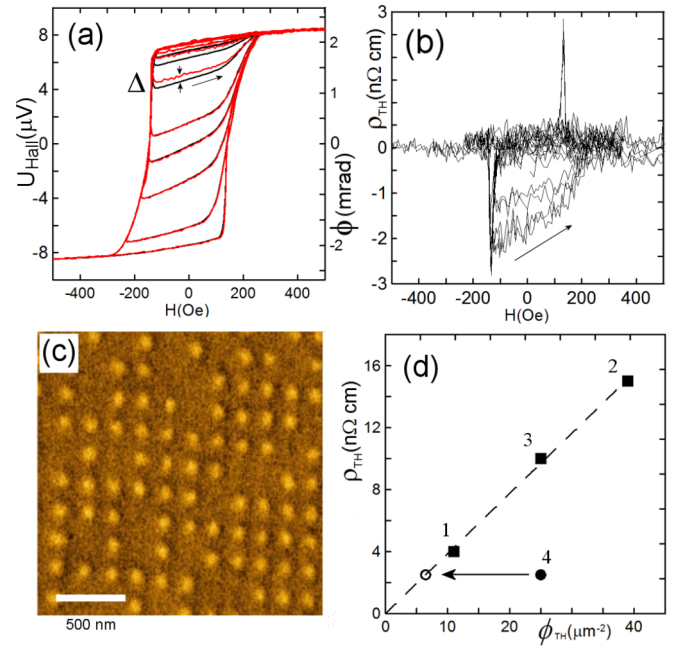


FIG. 7. (a) MOKE (red line) and Hall (black line) hysteresis loops plotted on the same scale for sample 4 ($50 \times 50 \mu\text{m}^2$ Hall cross). (b) Hysteresis curve of the topological Hall effect. The arrow denotes minor loop. (c) MFM image for the remanent state. (d) Dependence of the THE on the value of the irradiated spot density in the system. The squares are for the samples with concentric distribution of the irradiation fluence in the spot (samples 1–3). The linear dependence passing through zero indicates the skyrmionic topological nature of the magnetic bubbles. Black circle is for sample 4. White circle corresponds to the estimated density of the skyrmions in sample 4, which is $\sim 1/4$ of the irradiated spot density in this case.

ferromagnetic metals. Indeed adiabaticity parameter $a = \omega_R \tau = \omega_{RD}/V_F \approx 5 \times 10^{14} \times 0.5 \times 10^{-7}/2 \times 10^6 \approx 10$.

Here d is the skyrmion size and V_F is Fermi speed. The typical measured value of the THE in FeGe is 80 n Ω cm [31] to 136 n Ω cm [32], or 0.4 n Ω cm per skyrmion/ μm^2 to 0.68 n Ω cm per skyrmion/ μm^2 , which is also close to the value of the effect we obtained. The characteristic value of the THE in the A phase of MnSi is noticeably less and is 4.5–40 n Ω cm [8,33]. Perhaps this is due to the noticeably smaller size of skyrmions ($d = \lambda/2 = 9$ nm) and the exchange constant value, which leads to violation of adiabatic conditions and a decrease in the magnitude of the effect.

It is easy to estimate the magnitude of the topological field arising in our system using the relation $B = \Phi_0 \psi$, where $\Phi_0 = hc/e_0 = 40$ G μm^2 . So the topological fields are within 400–1600 G in our structures. The coefficient of the ordinary Hall effect R_0 in Co/Pt films has a very small value of about $0.5\text{--}1 \times 10^{-3}$ m Ω cm/G. The use of this value for estimating the THE in our system yields effect values that are an order of magnitude smaller than those observed experimentally. Such a significant discrepancy between simple estimates of THE [34,35] and experimental values was previously observed in transition metal films [10]. As discussed in Ref. [10] in detail, the topological Hall coefficient can significantly exceed the ordinary Hall coefficient for thin films of transition metals. The use of R_0 for the direct estimation of the THE

should work well for single-band materials, while transition ferromagnets have several active electron and hole bands. In this case, the ordinary Hall effect is suppressed, since the contributions of electrons and holes cancel each other. On the contrary, due to the fact that the Berry phase can act differently on charge carriers from different bands, the topological effect does not decrease.

Although our LTEM images demonstrate pure Bloch-type skyrmions, this method does not allow us to determine the real helicity of the skyrmions appearing in our samples. This is because the Néel component of the domain does not contribute to the contrast of the images. In this regard, we want to point out the following circumstances. (i) The THE does not depend on the helicity of skyrmions and is the same for both Bloch and Néel and intermediate twisted skyrmions. (ii) Sufficiently high values of the DMI are required to stabilize pure Néel skyrmions ($1\text{--}2\text{ mJ/m}^2$) [36,37]. This can be achieved in three-layer structures, when the ferromagnetic layer is surrounded by two different heavy metals, so that the DMIs at both interfaces have the same sign. For example, Pt/Co/Ir [34,35] or Ir/Fe/Co/Pt [10] are such systems. In the case of a symmetric Pt/Co/Pt structure, the DMIs at opposite interfaces have opposite signs also, canceling each other. In our initial films, we observe an ordinary labyrinth domain structure [Fig. 1(d)]. Magnetic bubbles (skyrmions) are stabilized due to the pinning effect in regions with a reduced anisotropy [24] in our case. It is highly likely that the DMI is also present in our system [38] and the appearing skyrmions have a twisted structure (and they are not of pure Bloch type as shown in Fig. 6). But this does not affect in any way the observed THE. In addition, the schematic sequence of magnetic configurations shown in Fig. 6 should also remain the same in the case of twisted skyrmions.

An additional sample, sample 4, with uniformly reduced anisotropy in the spot is studied for comparison. Only a part of the spots contains magnetic bubbles [Fig. 7(c)] in the remanent state of the sample. Micromagnetic simulations [23] demonstrate that the magnetization reversal begins with the magnetization turnover in the center of the spot in this case [Fig. 6(c)]. The process is less determined here and formation of both the topologically trivial onion states and topologically charged skyrmions are possible in different spots. While there are no evident steps in the Hall curve of sample 4 there is some difference between the minor Hall and MOKE loops. The corresponding value of the THE is $\Delta \sim 2.5\text{ n}\Omega\text{ cm}$. It is four times less than the THE in sample 3, which has the same density of the irradiated spots in the lattices. This means that in the case of the uniformly irradiated spots only 1/4 of them contain magnetic bubbles which are skyrmions while the rest of the bubbles are topologically trivial. It should be noted that some of the points do not exhibit magnetic contrast in zero field. This fact indicates that the observed magnetic states are just magnetic bubbles, not magnetic vortices [22]. This also confirms that the used irradiation fluence equal to 2×10^{15} (Table I) reduces the value of perpendicular anisotropy, but does not make it easy plane.

Can the observed effects be explained not by the topological contribution to the transport measurements, but, for example, by the contribution of the magnetoresistance or other effects associated with the current through the regions

of inhomogeneous magnetization? It can be seen that the appearance of magnetic bubbles in itself does not lead to a difference in the magneto-optical and Hall signals [Sm point in Fig. 2(b)]. Similarly, sample 4 demonstrates the effect that is 4 times lower than the value that should follow from the estimate of the number of magnetic bubbles. So the nonuniform magnetization cannot explain the observed effects by itself. In principle, the contribution of magnetoresistance to the observed transport effects is not excluded. However this contribution is $\sim M^2$ and is an even effect in the external magnetic field. The same quadratic terms are possible in the magneto-optical response (the Vogt and Cotton-Mouton effects), but it makes no sense to discuss them in more detail, since we do not see even dependencies on the external field in the experiments. Could there be other contributions to the Hall signal that are not related to normal, anomalous, and topological Hall? In principle, they can be in media with a nonuniform distribution of magnetization. The contribution of inhomogeneous cubic terms to the conductivity tensor can be represented as

$$\sigma_{ik}^{(3)} = \gamma_{ikpqstn} M_p \partial_l M_q \partial_n M_s.$$

In this case, a lot of effects are possible, for example,

$$\begin{aligned} \sigma_{ik}^{(3)} = & \gamma_1 (\mathbf{M} \cdot [\partial_i \mathbf{M} \times \partial_n \mathbf{M}]) + \gamma_2 \mathbf{M} (\text{div } \mathbf{M})^2 \\ & + \gamma_3 \mathbf{M} (\text{rot } \mathbf{M})^2. \end{aligned}$$

However, only the first topological term has an exchange nature, since it is invariant with respect to the coherent rotation of the magnetic moments. All other contributions are of a spin-orbital nature. Since they contain the same order of the spatial derivative of the magnetization as the exchange topological term, they are small compared to it.

In summary, we estimated the value of the topological magneto-optic effect at the optical frequencies and showed that it should be 10^2 to 10^4 times less than the topological Hall effect in the same system. We did this by using that fact the THE in Co/Pt multilayers was measured by comparing Hall and magneto-optic Kerr effect loops obtained in the same run. Specially designed nanostructured samples were used to obtain dense lattices of the magnetic bubbles with the predetermined density. The observed THE was proportional to the skyrmion density in the system. We also want to mention here that while the topological magneto-optic effect at the optical frequencies is negligible, it should be resonantly large at the frequencies corresponding to the exchange interaction energy.

We are grateful to Dr. O. G. Udalov for a fruitful discussion. This research was supported by the Russian Science Foundation (Grant No. 18-72-10026). Partial support was provided under Grant No. 18-29-27018 (MFM measurements). The samples were irradiated with the use of the equipment of Interdisciplinary Resource Centre for Nanotechnology of Saint Petersburg State University. The facilities of the center ‘‘Physics and Technology of Micro- and Nanostructures’’ at IPM RAS were used for the analysis of the samples. The equipment of CIC nanoGUNE BRTA (San Sebastian, Spain) was used for performing LTEM measurements.

- [1] Y. Aharonov and A. Stern, Origin of the Geometric Forces Accompanying Berry's Geometric Potentials, *Phys. Rev. Lett.* **69**, 3593 (1992).
- [2] P. Bruno, V. K. Dugaev, and M. Taillefumier, Topological Hall Effect and Berry Phase in Magnetic Nanostructures, *Phys. Rev. Lett.* **93**, 096806 (2004).
- [3] A. Fert, The origin, development and future of spintronics, Nobel Lecture 2007, https://www.nobelprize.org/uploads/2017/07/fert_lecture-1.pdf.
- [4] S. Mühlbauer, B. Binz, F. Jonietz, C. Pfleiderer, A. Rosch, A. Neubauer, R. Georgii, and P. Boni, Skyrmion lattice in a chiral magnet, *Science* **323**, 915 (2009).
- [5] S. Heinze, K. von Bergmann, M. Menze, J. Brede, A. Kubetzka, R. Wiesendanger, G. Bihlmayer, and S. Blugel, Spontaneous atomic-scale magnetic skyrmion lattice in two dimensions, *Nat. Phys.* **7**, 713 (2011).
- [6] A. Bogdanov and A. Hubert, Thermodynamically stable magnetic vortex states in magnetic crystals, *J. Magn. Magn. Mater.* **138**, 255 (1994).
- [7] I. Dzyaloshinskii and B. Ivanov, Localized topological solitons in a ferromagnet, *Pis'ma Zh. Eksp. Teor. Fiz.* **29**, 592 (1979) [*JETP Lett.* **29**, 540 (1979)].
- [8] A. Neubauer, C. Pfleiderer, B. Binz, A. Rosch, R. Ritz, P. G. Niklowitz, and P. Boni, Topological Hall Effect in the A Phase of MnSi, *Phys. Rev. Lett.* **102**, 186602 (2009).
- [9] M. He, G. Li, Z. Zhu, Y. Zhang, L. Peng, R. Li, J. Li, H. Wei, T. Zhao, X.-G. Zhang, S. Wang, S.-Z. Lin, L. Gu, G. Yu, J. W. Cai, and B. Shen, Evolution of topological skyrmions across the spin reorientation transition in Pt/Co/Ta multilayers, *Phys. Rev. B* **97**, 174419 (2018).
- [10] M. Raju, A. Yagil, A. Soumyanarayanan, A. K. C. Tan, A. Almoalem, F. Ma, O. M. Auslaender, and C. Panagopoulos, The evolution of skyrmions in Ir/Fe/Co/Pt multilayers and their topological Hall signature, *Nat. Commun.* **10**, 696 (2019).
- [11] Y. Ohuchi, Y. Kozuka, M. Uchida, K. Ueno, A. Tsukazaki, and M. Kawasaki, Topological Hall effect in thin films of the Heisenberg ferromagnet EuO, *Phys. Rev. B* **91**, 245115 (2015).
- [12] J. C. Gallagher, K. Y. Meng, J. T. Brangham, H. L. Wang, B. D. Esser, D. W. McComb, and F. Y. Yang, Robust Zero-Field Skyrmion Formation in FeGe Epitaxial Thin Films, *Phys. Rev. Lett.* **118**, 027201 (2017).
- [13] C. Liu, Y. Zang, W. Ruan, Y. Gong, K. He, X. Ma, Q.-K. Xue, and Y. Wang, Dimensional Crossover-Induced Topological Hall Effect in a Magnetic Topological Insulator, *Phys. Rev. Lett.* **119**, 176809 (2017).
- [14] A. Gerber, Interpretation of experimental evidence of the topological Hall effect, *Phys. Rev. B* **98**, 214440 (2018).
- [15] K. M. Fijalkowski, M. Hartl, M. Winnerlein, P. Mandal, S. Schreyeck, K. Brunner, C. Gould, and L. W. Molenkamp, Coexistence of Surface and Bulk Ferromagnetism Mimics Skyrmion Hall Effect in a Topological Insulator, *Phys. Rev. X* **10**, 011012 (2020).
- [16] J. Matsuno, N. Ogawa, K. Yasuda, F. Kagawa, W. Koshihara, N. Nagaosa, Y. Tokura, and M. Kawasaki, Interface driven topological Hall effect in SrRuO₃-SrIrO₃ bilayer, *Sci. Adv.* **2**, e1600304 (2016).
- [17] Y. Ohuchi, J. Matsuno, N. Ogawa, Y. Kozuka, M. Uchida, Y. Tokura, and M. Kawasaki, Electric-field control of anomalous and topological Hall effects in oxide bilayer thin films, *Nat. Commun.* **9**, 213 (2018).
- [18] K. S. Denisov, I. V. Rozhansky, N. S. Averkiev, and E. Lähderanta, General theory of the topological Hall effect in systems with chiral spin textures, *Phys. Rev. B* **98**, 195439 (2018).
- [19] O. G. Udalov, Skew scattering of cold unpolarized neutrons in ferromagnetic crystal, *J. Phys. Soc. Jpn.* **82**, 064714 (2013).
- [20] K. S. Denisov, I. V. Rozhansky, N. S. Averkiev, and E. Lähderanta, Electron Scattering on a Magnetic Skyrmion in the Nonadiabatic Approximation, *Phys. Rev. Lett.* **117**, 027202 (2016).
- [21] A. G. Gurevich and G. A. Melkov, *Magnetization Oscillations and Waves* (CRC Press, New York, 1996).
- [22] M. V. Sapozhnikov, S. N. Vdovichev, O. L. Ermolaeva, N. S. Gusev, A. A. Fraerman, S. A. Gusev, and Yu. V. Petrov, Artificial dense lattice of magnetic bubbles, *Appl. Phys. Lett.* **109**, 042406 (2016).
- [23] M. V. Sapozhnikov, Y. V. Petrov, N. S. Gusev, A. G. Temiryazev, O. L. Ermolaeva, V. L. Mironov and O. G. Udalov, Artificial Dense Lattices of Magnetic Skyrmions, *Materials* **13**, 99 (2020).
- [24] M. V. Sapozhnikov, Skyrmion lattice in a magnetic film with spatially modulated material parameters, *J. Magn. Magn. Mater.* **396**, 338 (2015).
- [25] L. H. Li and Y. Chen, Electric contributions to magnetic force microscopy response from graphene and MoS₂ nanosheets, *J. Appl. Phys.* **116**, 213904 (2014).
- [26] L.-C. Peng, Y. Zhang, S.-L. Zuo, M. He, J.-W. Cai, S.-G. Wang, H.-X. Wei, J.-Q. Li, T.-Y. Zhao, and B.-G. Shen, Lorentz transmission electron microscopy studies on topological magnetic domains, *Chin. Phys. B* **27**, 066802 (2018).
- [27] M. de Graef, 2. Lorentz microscopy: Theoretical basis and image simulations, *Exp. Methods Phys. Sci.* **36**, 27 (2001).
- [28] X. Zhang, J. Xia, Y. Zhou, D. Wang, X. Liu, W. Zhao, and M. Ezawa, Control and manipulation of a magnetic skyrmionium in nanostructures, *Phys. Rev. B* **94**, 094420 (2016).
- [29] A. G. Kolesnikov, M. E. Stebliy, A. S. Samardak, and A. V. Ognev, Skyrmionium: High velocity without the skyrmion Hall effect, *Sci. Rep.* **8**, 16966 (2018).
- [30] X. Z. Yu, N. Kanazawa, Y. Onose, K. Kimoto, W. Z. Zhang, S. Ishiwata, Y. Matsui, and Y. Tokura, Near room-temperature formation of a skyrmion crystal in thin-films of the helimagnet FeGe, *Nat. Mater.* **10**, 106 (2011).
- [31] S. X. Huang and C. L. Chien, Extended Skyrmion Phase in Epitaxial FeGe(111) Thin Films, *Phys. Rev. Lett.* **108**, 267201 (2012).
- [32] N. A. Porter, J. C. Gartside, and C. H. Marrows, Scattering mechanisms in textured FeGe thin films: Magnetoresistance and the anomalous Hall effect, *Phys. Rev. B* **90**, 024403 (2014).
- [33] R. Ritz, M. Halder, C. Franz, A. Bauer, M. Wagner, R. Bamler, A. Rosch, and C. Pfleiderer, Giant generic topological Hall resistivity of MnSi under pressure, *Phys. Rev. B* **87**, 134424 (2013).
- [34] D. Maccariello, W. Legrand, N. Reyren, K. Garcia, K. Bouzehouane, S. Collin, V. Cros, and A. Fert, Electrical detection of single magnetic skyrmions in metallic multilayers at room temperature, *Nat. Nanotechnol.* **13**, 233 (2018).

- [35] K. Zeissler, S. Finizio, K. Shahbazi, J. Massey, F. Al Ma'Mari, D. M. Bracher, A. Kleibert, M. C. Rosamond, E. H. Linfield, T. A. Moore, J. Raabe, G. Burnell, and C. H. Marrows, Discrete Hall resistivity contribution from Néel skyrmions in multilayer nanodiscs, *Nat. Nanotechnol.* **13**, 1161 (2018).
- [36] S. Castillo-Sepúlveda, R. M. Corona, A. S. Núñez, and D. Altbir, Twisted skyrmions through dipolar interactions, *J. Magn. Magn. Mater.* **484**, 451 (2019).
- [37] A. Bernand-Mantel, C. B. Muratov, and T. M. Simon, Unraveling the role of dipolar versus Dzyaloshinskii-Moriya interactions in stabilizing compact magnetic skyrmions, *Phys. Rev. B* **101**, 045416 (2020).
- [38] N. S. Gusev, A. V. Sadovnikov, S. A. Nikitov, M. V. Sapozhnikov, and O. G. Udalov, Manipulation of the Dzyaloshinskii-Moriya Interaction in Co/Pt Multilayers with Strain, *Phys. Rev. Lett.* **124**, 157202 (2020).